Materials Science in Semiconductor Processing 29 (2015) 95–101

Contents lists available at ScienceDirect

Materials Science in Semiconductor Processing

journal homepage: www.elsevier.com/locate/mssp

Advantage of InGaN-based light-emitting diodes with trapezoidal electron blocking layer

Tian-Hu Wang [a], Jin-Liang Xu [b,*]

[a] Beijing Key Laboratory of New and Renewable Energy, North China Electric Power University, Beijing 102206, China
[b] Beijing Key Laboratory of Multiphase Flow and Heat Transfer for Low Grade Energy, North China Electric Power University, Beijing 102206, China

ARTICLE INFO

Available online 13 November 2013

Keywords:
Light-emitting diodes
Electron blocking layer
Efficiency droop
Electron leakage

ABSTRACT

In this study, a trapezoidal-shaped electron blocking layer is proposed to improve efficiency droop of InGaN/GaN multiple quantum well light-emitting diodes. The energy band diagram, carrier distribution profile, electrostatic field, and electron current leakage are systematically investigated between two light-emitting diodes with different electron blocking layer structures. The simulation results show that, when traditional AlGaN electron blocking layer is replaced by trapezoidal-shaped electron blocking layer, the electron current leakage is dramatically reduced and the hole injection efficiency in markedly enhanced due to the better polarization match, the quantum-confined Stark effect is mitigated and the radiative recombination rate is increased in the active region subsequently, which are responsible for the alleviation of efficiency droop. The optical performance of light-emitting diodes with trapezoidal-shaped electron blocking layer is significantly improved when compared with its counterpart with traditional AlGaN electron blocking layer.

1. Introduction

In recent decade, InGaN-based light-emitting diodes (LEDs) have become available and been investigated comprehensively due to their advantages of compact size, long lifetime, environment-friendly and low power consumption, they have potential applications in full-color outdoor displays, back lighting of liquid crystal displays and solid-state lighting, the conventional incandescent and fluorescent lamps will be replaced by this “green light source” in the future [1–3]. However, further development of high efficiency and high power solid-state lighting is restricted by the problem called “efficiency droop”, which must be solved for LED operating at high injection currents [4–6]. In order to improve the LED efficiency, many efforts have been made to explain the mechanism of efficiency droop, which includes electron leakage [5,6], lack of hole injection [7,8], non-uniform distribution of carriers [9,10], quantum-confined Stark effect in multiple quantum wells (MQWs) [11], Auger recombination [12], carrier delocalization [13], defects [14], self-heating effect [15], etc. A comprehensive discussion of different mechanisms for efficiency droop has also been published recently [4]. However, the physical origin of efficiency droop is still under debate now.

Among above mechanisms, it has been generally accepted that electron overflow out of the active region and insufficient hole injection efficiency are the main responsible mechanisms for efficiency droop [5–10,16–18]. To reduce electron leakage and enhance hole injection efficiency, many LED structure design and optimization works have been made, which can be summarized as quantum well design [11,19–21], quantum barrier design [3,5,6,9,10,22–24], last barrier design [25–28], and electron blocking layer (EBL) design [3,5,8,16,29–41]. Specially, among these works, electron blocking layer plays an important role in carrier transport properties. The electron

* Corresponding author. Tel./fax: +86 10 61772268.
E-mail address: xjl@ncepu.edu.cn (J.-L. Xu).

1369-8001/$ - see front matter © 2013 Elsevier Ltd. All rights reserved.
http://dx.doi.org/10.1016/j.mssp.2013.10.026

in nitride-based material has relatively low effective mass and thus a high mobility [16], causing that it can spill over the active region into the p-type layer easily to recombine with hole via non-radiative process. When an AlGaN electron blocking layer is inserted between the active layer and the p-type layer, the electron escaping from the active region can be suppressed. On the other hand, however, when the EBL is used, the injection of hole becomes difficult due to low mobility caused by hole's high effective mass, low p-type doping efficiency in EBL, and downward band-bending caused by polarization near the EBL [29].

In order to develop the performance of electron blocking layer, lots of EBL structures are proposed which can be classified as following: AlGaInN EBL [3,5], InAlN EBL [16], step-shaped EBL [29–31], graded EBL [32,33], superlattice EBL [34–36], *n*-type EBL [37,38], and removing the AlGaN EBL [39–41]. These designs have been demonstrated to be effective for improving the efficiency droop. However, there are still some limitations for these designs such as difficulties of realization in epitaxial growth, the degraded crystal quality of subsequent p-type layer, not effective suppression of electron due to residual polarization, sometimes the electron suppression and hole injection cannot be enhanced synchronously due to the EBL's "double-edged sword" characteristic. In this paper, different from above designs, a trapezoidal-shaped EBL with gradually-increased/constant/gradually-decreased Al composition is designed. This concept comes from the energy band engineering expecting to obtain improved lattice-match status around the EBL. The improved hole injection efficiency and enhanced electron confinement ability for this redesigned EBL, as well as the subsequent alleviated quantum-confined Stark effect in active region are justified numerically in detail.

2. Device structure and parameters

Two LED structures were designed in this study for comparison. LED A used as the reference structure was prepared on a c-plane sapphire substrate. Between the substrate and active region, a 50-nm-thick un-doped GaN buffer layer was deposited followed by a 3-μm-thick n-type GaN layer (n-doping$=5\times10^{18}$ cm^{-3}). The active region was composed of five pairs of InGaN/GaN quantum wells (five 2.2-nm-thick $In_{0.11}Ga_{0.89}N$ wells separated by six 15-nm-thick GaN barriers). On top of the active region were a 30-nm-thick p-type $Al_{0.15}Ga_{0.85}N$ EBL (p-doping$=1.2\times10^{18}$ cm^{-3}) followed by a 250-nm-thick p-type GaN cap layer (p-doping$=1.2\times10^{18}$ cm^{-3}). The device geometry was 300×300 μm^2. LED B is designed identically to LED A except that the convention AlGaN EBL was replaced by a p-type trapezoidal $Al_xGa_{1-x}N$/AlGaN/$Al_yGa_{1-y}N$ EBL (p-doping$=1.2\times10^{18}$ cm^{-3}). Al composition x was gradually increased from 0 to 15% along the grown direction in $Al_xGa_{1-x}N$ layer, composition y was gradually decreased from 15% to 0 in the $Al_yGa_{1-y}N$ EBL layer, composition was kept as constant value of 15% in the middle AlGaN layer. The thickness of each layer is 10 nm. Fig. 1 shows the schematic diagrams of the two LED structures, the energy band schematic diagrams of EBLs are also illustrated in the right-hand of Fig. 1.

3. Theory

The optical and electric characteristics of two LEDs were studied by APSYS simulation program [42] (developed by Crosslight Software Inc.), which self-consistently solves the Poisson's equation, current continuity equations, carrier transport equations, photon rate equation, and quantum mechanical wave equations. The polarization charge caused by spontaneous and piezoelectric polarization effect is calculated by the method reported by Fiorentini et al. [43]. The spontaneous polarization of the ternary nitride alloys can be expressed as

$$P_{sp}(In_xGa_{1-x}N) = -0.0413x - 0.0339(1-x) + 0.0378x(1-x), \quad (1)$$

$$P_{sp}(Al_xGa_{1-x}N) = -0.0898x - 0.0339(1-x) + 0.0191x(1-x) \quad (2)$$

The piezoelectric polarization of ternary alloys can be expressed as

$$P_{pz}(In_xGa_{1-x}N) = P_{pz}(InN)x + P_{pz}(GaN)(1-x), \quad (3)$$

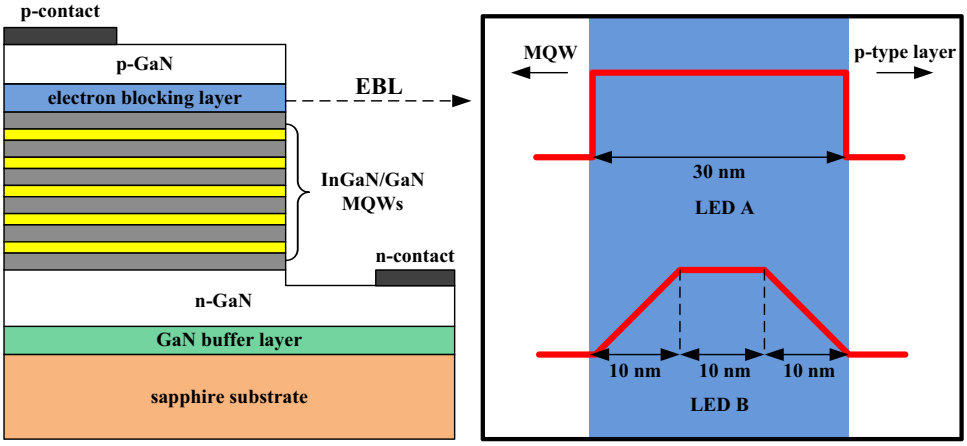

Fig. 1. Schematic diagrams of the two LED structures.

$$P_{pz}(Al_xGa_{1-x}N) = P_{pz}(AlN)x + P_{pz}(GaN)(1-x), \quad (4)$$

where

$$P_{pz}(InN) = -1.373\varepsilon + 7.559\varepsilon^2, \quad (5)$$

$$P_{pz}(GaN) = -0.918\varepsilon + 9.541\varepsilon^2, \quad (6)$$

$$P_{pz}(AlN) = -1.808\varepsilon + 5.642\varepsilon^2 (\varepsilon < 0), \quad (7)$$

$$P_{pz}(AlN) = -1.808\varepsilon - 7.888\varepsilon^2 (\varepsilon > 0). \quad (8)$$

The basal strain for the alloy matched to the GaN layer is defined as

$$\varepsilon = \frac{(a_{sub} - a)}{a}, \quad (9)$$

where a_{sub} and a are the lattice constants of the GaN and alloy layers, respectively. The total polarization is the sum of the spontaneous and piezoelectric polarization.

The band gap energies of $In_xGa_{1-x}N$ and $Al_xGa_{1-x}N$ ternary alloys are calculated by the formulas expressed in Ref. [44]. For InN, GaN, and AlN, the band gap energy as a function of temperature T can be expressd by the Varshni formula [44]:

$$E_g(T) = E_g(0) - \frac{\alpha T^2}{T+\beta}, \quad (10)$$

where $E_g(T)$ is the band gap energy at temperature T, $E_g(0)$ is the band gap energy at 0 K, α and β are material related constants. The values of E_g (0), α, and β for InN are 0.735 eV, 0.245 meV/K, and 624 K, respectively. The values for GaN are 3.507 eV, 0.909 meV/K, 830 K, respectively. The values for AlN are 6.23 eV, 1.799 meV/K, 1462 K, respectively. The temperature is set to be 300 K in the simulation. For ternary alloys of InGaN and AlGaN, the band gap energies can be expressed as follows [44]:

$$E_g(In_xGa_{1-x}N) = E_g(InN)x + E_g(GaN)(1-x) - b(In_xGa_{1-x}N)x(1-x), \quad (11)$$

$$E_g(Al_xGa_{1-x}N) = E_g(AlN)x + E_g(GaN)(1-x) - b(Al_xGa_{1-x}N)x(1-x), \quad (12)$$

where E_g ($In_xGa_{1-x}N$) and E_g ($Al_xGa_{1-x}N$) are the band gap energies of $In_xGa_{1-x}N$ and $Al_xGa_{1-x}N$, the bowing parameters for $In_xGa_{1-x}N$ and $Al_xGa_{1-x}N$ are 1.43 and 1.0, respectively. APSYS employs the 6×6 kp model to caculate the energy band structures, which was developed by Chuang and Chang [45,46]. Other material parameters of the relevant semiconductors are cited from Ref. [44].

The Caughey-Thomas approximation is employed in this study to calculate the electron and hole mobilities which can be expressed as [47]

$$\mu_i(N) = \mu_{min,i} + \frac{\mu_{max,i} - \mu_{min,i}}{1.0 + (N/N_{ref,i})^{\alpha,i}}, \quad (13)$$

where i denotes either electron or hole, μ_{min}, μ_{max}, N_{ref}, and α are experimental fitting parameters. For electron in $In_xGa_{1-x}N$ ternary alloy, the values of μ_{min}, μ_{max}, N_{ref}, and α are 684 $cm^2/V\,s$, 386 $cm^2/V\,s$, 1.0×10^{17} cm^{-3}, and 1.37, respectively. For electron in $Al_xGa_{1-x}N$ ternary alloy, the values are 306 $cm^2/V\,s$, 132 cm^2/Vs, 1.0×10^{17} cm^{-3}, and 0.29, respectively. For hole in $In_xGa_{1-x}N$ alloy, the values of μ_{min}, μ_{max}, N_{ref}, and α are 2 $cm^2/V\,s$, 2 $cm^2/V\,s$, 2.75×10^{17} cm^{-3}, and 0.395, respectively. In $Al_xGa_{1-x}N$ alloy, the values are 2 $cm^2/V\,s$, 2 $cm^2/V\,s$, 3.0×10^{17} cm^{-3}, and 0.395, respectively.

The non-radiative recombination processes and current leakage are taken into account. The Shockley-Read-Hall (SRH) recombination lifetime is set to be 100 ns. The internal absorption within the LED device and the light

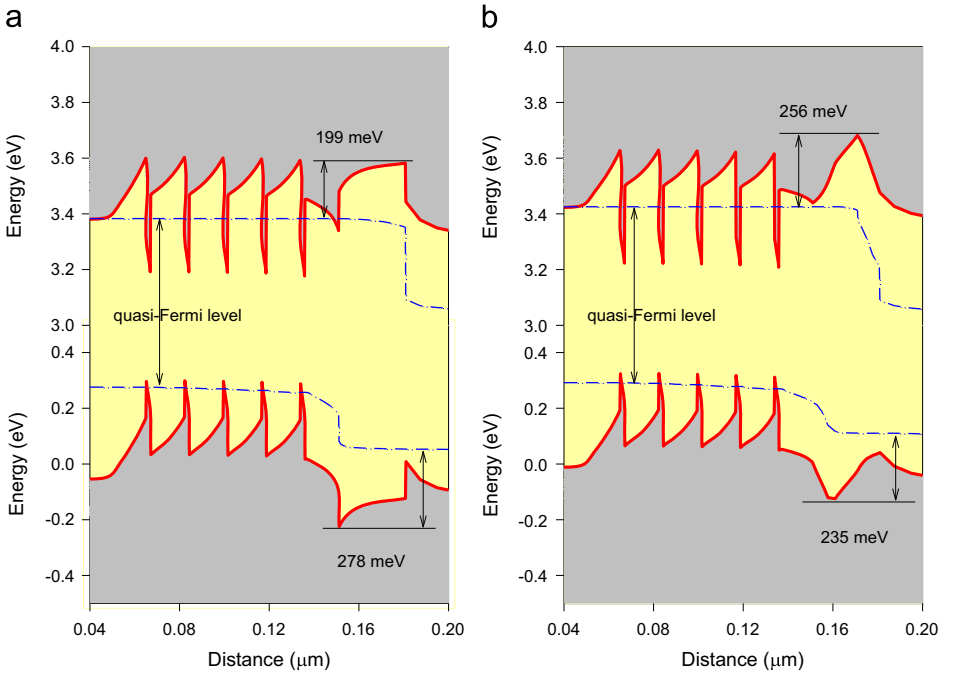

Fig. 2. Energy band diagrams for (a) LED A and (b) LED B at injection current of 150 mA.

extraction efficiency are assumed to 500 m^{-1} and 78%, respectively. Other simulation parameters used in this paper are cited from our previous paper Ref. [48], in which the model validation has been performed, more details can be found in Ref. [48].

4. Results and discussion

Fig. 2 shows the energy band diagrams of LEDs A and B at injection current of 150 mA. The effective potential barrier of EBL concept is an useful tool to evaluate the electron confinement ability and hole injection efficiency for EBL, which is defined as the potential difference between the conduction band edge (valence band edge) and its relative quasi-Fermi level in front of it. It can be seen from Fig. 2(a) that, the energy band of last barrier is downward band-bending seriously due to the high polarization mismatch between last barrier and conventional AlGaN EBL, and there exists a low energy point below the quasi-Fermi level at the last barrier/EBL interface in the conduction band. Consequently, the effective potential barrier of EBL is small, leading to that the electrons cannot be confined effectively and hence overflow to the p-type layer easily. Because of better lattice match when trapezoidal EBL is used, the downward band-bending of last barrier is improved and the low energy point is lifted to be above the quasi-Fermi level. Therefore, the effective potential barrier increases from 199 meV to 256 meV, indicating the enhanced electron confinement ability. On the other hand, the polarization-induced band-bending in the valence band causes a spike at the last barrier/EBL interface for LED A, the hole will suffer from a obstacle potential barrier at the spike, which thus limits the hole injection into the MQWs. On the contrary, the spike in LED B is alleviated so that the effective barrier height in valence band is reduced from 278 meV to 235 meV, which is beneficial for hole injection into the QWs. This improved status for EBL in the valence band is attributed to better polarization match at the last barrier/EBL interface when trapezoidal EBL is introduced.

Fig. 3 shows the electron concentration distribution around the active region and electron current leakage near the EBL at injection current of 150 mA. The electrons are injected form n-type layer into the active region and recombine with holes in the QWs, thus the vertical electron current density becomes smaller and smaller along the growth direction, the electrons which cannot be recombine with holes in the QWs and overflow to the p-type layer are defined as electron current leakage. It is consistent with the band diagrams that, the electron current leakage is so serious in LED A due to the polarization-induced small effective potential barrier in conduction band. When the EBL is replaced by trapezoidal EBL, the electron current leakage is significantly alleviated

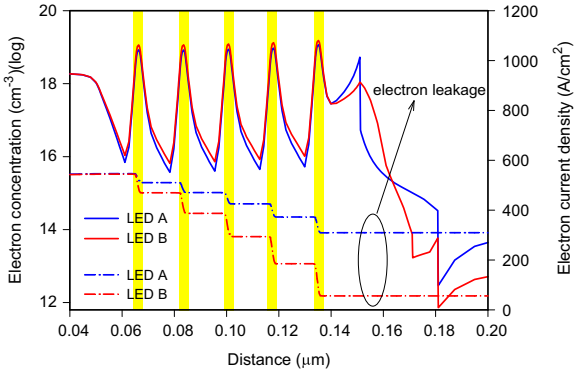

Fig. 3. Electron concentration and vertical electron current density of LEDs A and B at injection current of 150 mA.

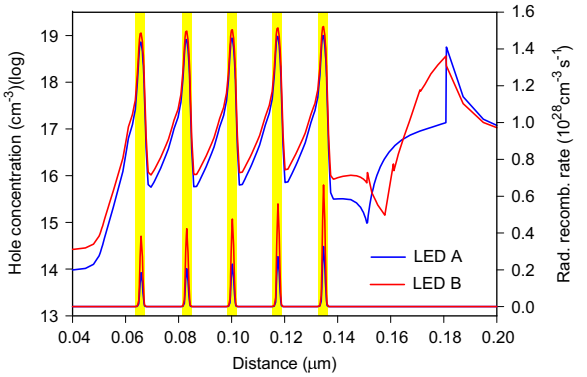

Fig. 4. Hole concentration and radiative recombination rate of LEDs A and B at injection current of 150 mA.

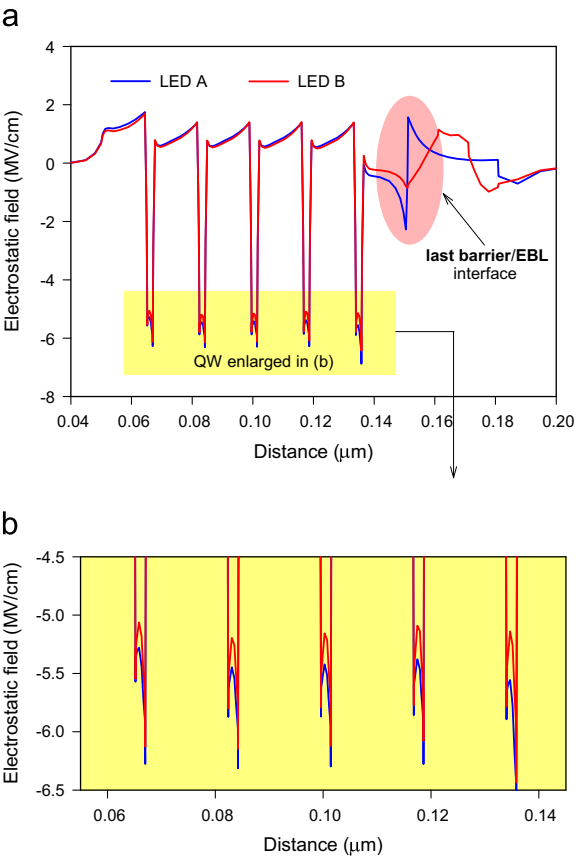

Fig. 5. Electrostatic field in the active region and around the EBL of LEDs A and B at injection current of 150 mA.

due to high effective potential barrier of EBL, which justify the enhanced electron confinement ability of EBL. Therefore, when compared with LED A, the electron concentration in every QW of LED B is increased, and electron concentration in p-type layer is also decreased as illustrated in Fig. 3.

Fig. 4 shows the hole concentration distribution and radiative recombination rate in the active region. Holes are injected from p-type layer into the QWs, the overflowed electrons in the p-type layer can capture holes before they approach the edge of active region, deteriorating the hole injection efficiency. Therefore, when electron current leakage is reduced, more holes can be injected into active region to participating in radiative recombination. Besides, the reduced obstacle potential barrier in valence band of LED B can also improve hole injection efficiency. Increased carrier concentration in active region leads to enhanced radiative recombination rate, which is clearly indicated in Fig. 4. The total radiative recombination rate for LED B is enhanced by a factor of 2.05, when compared with LED A.

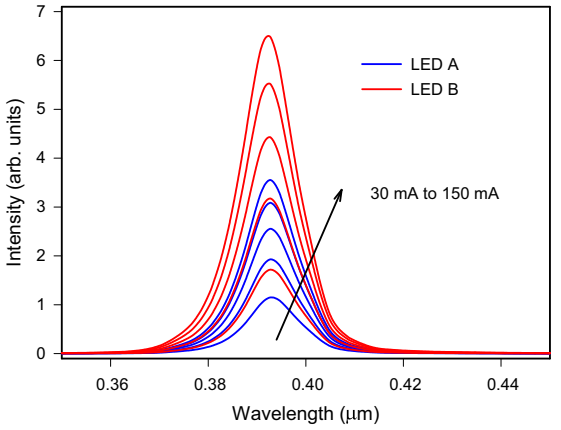

Fig. 6. Emission spectra of LEDs A and B in the injection current range from 30 mA to 150 mA.

The above mentioned advantage of LED B with trapezoidal EBL can be justified by the electrostatic field near the EBL, which is illustrated in Fig. 5 at injection current of 150 mA. It indicates that there is a much stronger electrostatic field at the last barrier/EBL interface of LED A caused by lattice-mismatch-induced surface charge. This field will decrease the effective potential barrier for electron in the conduction band and increase the effective barrier potential barrier for hole in the valence band, which thus aggravate electron leakage and impede hole injection into QWs. When trapezoidal EBL is used, the electrostatic field becomes weaker, it alleviates the band-bending situation at the last barrier/EBL interface. The electrostatic fields in each QW have been enlarged in Fig. 5(b) for easy comparison. The quantum-confined Stark effect in the quantum wells induced by the internal electric field can deteriorate the wave function spatial overlap between electrons and holes, which thus decreases radiative recombination rate and the internal quantum efficiency. Due to the screening effect of carriers confined in MQWs, the polarization in active region of LED B is smaller than that of LED A when the carrier concentration is increased, leading to the reduced electrostatic fields in each QW of LED B. Therefore, the overlap of electron and hole wave function can be enhanced due to the reduced quantum-confined Stark effect, which improves the radiative recombination rate in active region.

Fig. 6 shows the emission spectra of LEDs A and B in the injection current range from 30 mA to 150 mA, respectively. In indicates that the emission intensity of LED B is enhanced than that of LED A at the same injection current, and the enhanced degree increases with the injection current increased. The intensity of LED B is enhanced by a factor of 1.5 than that of LED A at 30 mA. When the injection current increases to 150 mA the factor increases to 1.8. The improved intensity justifies that the radiative recombination rate in the active region was significantly enhanced due to the increased electron confinement, enhanced hole injection efficiency, and reduced quantum-confined Stark effect in MQWs.

Finally, the internal quantum efficiency and output power for LEDs A and B as a function of injection current

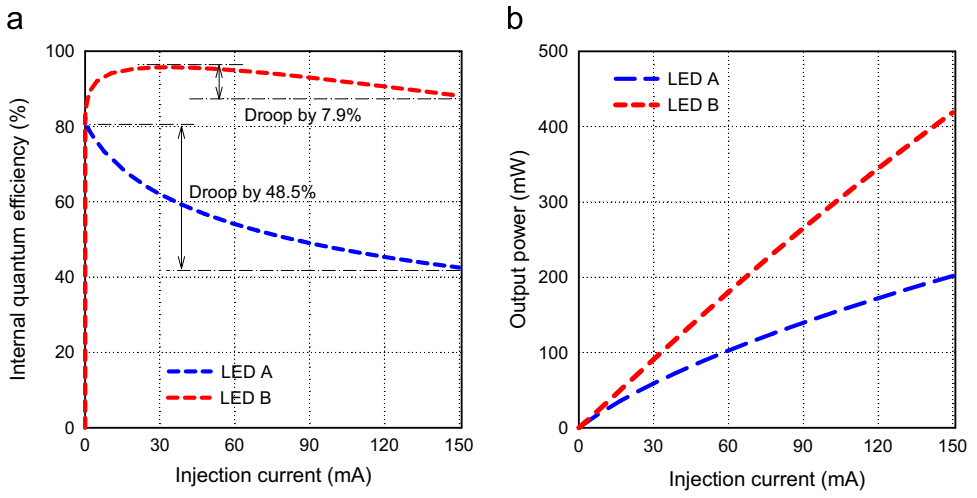

Fig. 7. Internal quantum efficiency and light output power of LEDs A and B as a function of injection current.

are depicted in Fig. 7. The overall characteristics of IQE and output power are both significantly improved for LED B, when compared with those of LED A. The percentage of efficiency droop (defined as $\eta=(IQE_{max}-IQE_{min})/IQE_{max}$, where IQE_{max} and IQE_{min} are the maximum and minimum internal quantum efficiencies, respectively) for LEDs A and B are 48.5% and 7.9%, respectively. This is attributed to the enhanced radiative recombination rate due to increased carrier concentration and reduced quantum-confined Stark effect in MQWs. When evaluating the optical performance of both LEDs A and B, the output power of LED B is 419 mW at injection current of 150 mA, which is about twice times higher than that of LED A.

It is noted that, the proposed structure in this study is an ideal structure. However, the experimental results for a real structure may include much complex phenomena such as the self-heating effect [5,15], crystal quality in the device growth process (e.g. crystalline quality of the AlGaN EBL layer with high Al mole fraction was usually degraded caused by the strain-induced defects [16]), interface roughness between layers [49], strain distribution in the active region (e.g. high optimum growth temperature for AlGaN EBL may produce some thermal damage on the active region [50]) and so on. Consequently, there may be some deviations between the simulation and experimental results. Although there are some deviations, it is believe that the simulation results can still provides a good guide for the structural design and optimization theoretically.

5. Conclusions

The trapezoidal electron blocking layer has been employed to reduce the efficiency droop. The lattice matched gradual varied Al composition in EBL reduce the polarization-charge mismatch between active region and EBL, thereby reducing the electric fields and the associated quantum-confined Stark effect. The better lattice match at the last barrier/EBL interface will alleviate polarization-induced band bending, which improves the EBL's performance in two ways. (1) It increases the effective potential barrier of conduction band, which can enhance electron confinement ability and reduce electron leakage. (2) The effective potential barrier in valence band is reduced, which is beneficial for hole injection into the active region. Consequently, carrier concentration in each quantum well is significantly increased. In addition, the quantum-confined Stark effect in the active region is also alleviated caused by screen effect of higher carrier concentration in the quantum wells. The joint effects of the increased carrier concentration and mitigated quantum-confined Stark effect in active region cause enhanced radiative recombination rate. As a result, the LED with trapezoidal electron blocking layer exhibits smaller efficiency droop and higher light output power.

Acknowledgments

This work was financially supported by the National Natural Science Foundation of China (U1034004 and 51210011).

References

[1] E.F. Schubert, J.K. Kim, Science 208 (2005) 1274–1278.
[2] M.R. Krames, O.B. Shchekin, R. Mueller-Mach, G.O. Mueller, L. Zhou, G. Harbers, M.G. Craford, IEEE J. Disp. Technol. 3 (2007) 160–175.
[3] Y.K. Kuo, M.C. Tsai, S.H. Yen, Opt. Commun. 282 (2009) 4252–4255.
[4] J. Piprek, Phys. Status Solidi A 207 (2010) 2217–2225.
[5] M.H. Kim, M.F. Schubert, Q. Dai, J.K. Kim, E.F. Schubert, J. Piprek, Y. Park, Appl. Phys. Lett. 91 (2007) 183507.
[6] M.F. Schubert, J. Xu, J.K. Kim, E.F. Schubert, M.H. Kim, S. Yoon, S.M. Lee, C. Sone, T. Sakong, Y. Park, Appl. Phys. Lett. 93 (2008) 041102.
[7] X. Ni, Q. Fan, R. Shimada, U.O. zgur, H. Morkoc, Appl. Phys. Lett. 93 (2008) 171113.
[8] S.H. Han, D.Y. Lee, S.J. Lee, C.Y. Cho, M.K. Kwon, S.P. Lee, D.Y. Noh, D. J. Kim, Y.C. Kim, S.J. Park, Appl. Phys. Lett. 94 (2009) 231123.
[9] Y.K. Kuo, T.H. Wang, J.Y. Chang, M.C. Tsai, Appl. Phsy. Lett 99 (2011) 091107.
[10] Y.K. Kuo, T.H. Wang, J.Y. Chang, Appl. Phys. Lett. 100 (2012) 031112.
[11] H.P. Zhao, G.Y. Liu, J. Zhang, J.D. Poplawsky, V. Dierolf, N. Tansu, Opt. Express 19 (2011) A991–A1007.
[12] Y.C. Shen, G.O. Mueller, S. Watanabe, N.F. Gardner, A. Munkholm, M. R. Krames, Appl. Phys. Lett. 91 (2007) 141101.
[13] J. Wang, L. Wang, W. Zhao, Z. Hao, Y. Luo, Appl. Phys. Lett. 97 (2010) 201112.
[14] B. Monemar, B.E. Sernelius, Appl. Phys. Lett. 91 (2007) 181103.
[15] A.A. Efremov, N.I. Bochkareva, R.I. Gorbunov, D.A. Lavrinovich, Y.T. Rebane, D.V. Tarkhin, Y.G. Shreter, Semiconductors 40 (2006) 605–610.
[16] S. Choi, H.J. Kim, S.S. Kim, J. Liu, J. Kim, J.H. Ryou, R.D. Dupuis, A. M. Fischer, F.A. Ponce, Appl. Phys. Lett. 96 (2010) 221105.
[17] Y.K. Kuo, J.Y. Chang, M.C. Tsai, S.H. Yen, Appl. Phys. Lett. 95 (2009) 011116.
[18] C.S. Xia, Z.M. Simon, Li, W. Lu, Z.H. Zhang, Y. Sheng, L.W. Cheng, Appl. Phys. Lett. 99 (2011) 233501.
[19] K. Ding, Y.P. Zeng, X.C. Wei, Z.C. Li, J.X. Wang, H.X. Lu, P.P. Cong, X.Y. Yi, G.H. Wang, J.M. Li, Appl. Phys. B 97 (2009) 465–468.
[20] S.H. Han, D.Y. Lee, H.W. Shim, G.C. Kim, Y.S. Kim, S.T. Kim, S.J. Lee, C. Y. Cho, S.J. Park, J. Phys. D: Appl. Phys 43 (2010) 354004.
[21] Y.J. Lee, C.H. Chen, C.J. Lee, IEEE Photon. Technol. Lett. 22 (2010) 1506–1508.
[22] J.Y. Chang, M.C. Tsai, Y.K. Kuo, Opt. Lett. 35 (2010) 1368–1370.
[23] M.C. Tsai, S.H. Yen, Y.K. Kuo, Appl. Phys. Lett. 98 (2011) 111114.
[24] C.H. Wang, S.P. Chang, P.H. Ku, J.C. Li, Y.P. Lan, C.C. Lin, H.C. Yang, H.C. Kuo, T.C. Lu, S.C. Wang, C.Y. Chang, Appl. Phys. Lett. 99 (2011) 171106.
[25] Y.K. Kuo, M.C. Tsai, S.H. Yen, T.C. Hsu, Y.J. Shen, IEEE J. Quantum Electron. 46 (2010) 1214–1220.
[26] S.H. Yen, M.L. Tsai, M.C. Tsai, S.J. Chang, Y.K. Kuo, IEEE Photon. Technol. Lett. 22 (2010) 1787–1789.
[27] Y.K. Kuo, Y.H. Shih, M.C. Tsai, J.Y. Chang, IEEE Photon. Technol. Lett. 23 (2011) 1630–1632.
[28] J. Chen, G.H. Fan, W. Pang, S.W. Zheng, Y.Y. Zhang, IEEE Photon. Technol. Lett. 24 (2012) 2218–2220.
[29] Y.K. Kuo, J.Y. Chang, M.C. Tsai, Opt. Lett. 35 (2010) 3285–3287.
[30] C.S. Xia, Z.M. Li, W. Lu, Z.H. Zhang, Y. Sheng, W.D. Hu, L.W. Cheng, J. Appl. Phys. 111 (2012) 094503.
[31] Y.K. Kuo, T.H. Wang, J.Y. Chang, J.D. Chen, IEEE Photon. Technol. Lett. 24 (2012) 1506–1508.
[32] C.H. Wang, C.C. Ke, C.Y. Lee, S.P. Chang, W.T. Chang, J.C. Li, Z.Y. Li, H.C. Yang, H.C. Kuo, T.C. Lu, S.C. Wang, Appl. Phys. Lett. 97 (2010) 261103.
[33] N. Zhang, Z. Liu, T. Wei, L. Zhang, X. Wei, X. Wang, H. Lu, J. Li, J. Wang, Appl. Phys. Lett. 100 (2012) 053504.
[34] R.B. Chung, C. Han, C.C. Pan, N. Pfaff, J.S. Speck, S.P. DenBaars, S. Nakamura, Appl. Phys. Lett. 101 (2012) 131113.
[35] Y.Y. Zhang, X.L. Zhu, Y.A. Yin, J. Ma, IEEE Electron Device Lett. 33 (2012) 994–996.
[36] C.S. Xia, Z.M. Simon Li, Z.Q. Li, Y. Sheng, Appl. Phys. Lett. 102 (2013) 013507.
[37] S.H. Yen, M.C. Tsai, M.L. Tsai, Y.J. Shen, T.C. Hsu, Y.K. Kuo, IEEE Photon. Technol. Lett. 21 (2009) 975–977.
[38] Y. Li, Y. Gao, M. He, J. Zhou, Y. Lei, L. Zhang, K. Zhu, Y. Chen, J. Disp. Technol. 9 (2013) 244–248.
[39] Y.A. Chang, J.Y. Chang, Y.T. Kuo, Y.K. Kuo, Appl. Phys. Lett. 100 (2012) 251102.
[40] Y.Y. Zhang, G.H. Fan, T. Zhang, IEEE J. Quantum Electron 48 (2012) 169–174.
[41] H.Y. Ryu, J.M. Lee, Appl. Phys. Lett. 102 (2013) 181115.

[42] APSYS by Crosslight Software Inc., Burnaby, Canada.
[43] V. Fiorentini, F. Bernardini, O. Ambacher, Appl. Phys. Lett. 80 (2002) 1204–1206.
[44] I. Vurgaftman, J.R. Meyer, J. Appl. Phys. 84 (2003) 3675–3696.
[45] S.L. Chuang, C.S. Chang, Phys. Rev. B 54 (1996) 2491–2504.
[46] S.L. Chuang, C.S. Chang, Semicond. Sci. Technol. 12 (1997) 252–263.
[47] C.M. Caughey, R.E. Thomas, Proc. IEEE 55 (1967) 2192–2193.
[48] J.L. Xu, T.H. Wang, Physica E 52 (2013) 8–13.
[49] Y.J. Liu, T.Y. Tsai, C.H. Yen, L.Y. Chen, T.H. Tsai, W.C. Liu, IEEE J. Quantum Electron 46 (2010) 492–498.
[50] W. Lee, J. Limb, J.H. Ryou, D. Yoo, T. Chung, R.D. Dupuis, J. Cryst. Growth 287 (2006) 577–581.